

Thermalization and free decay in Surface Quasi-Geostrophic flows

Tomas Teitelbaum¹ and Pablo D. Mininni^{1,2}

¹ *Departamento de Física, Facultad de Ciencias Exactas y Naturales,
Universidad de Buenos Aires and IFIBA, CONICET,
Ciudad Universitaria, 1428 Buenos Aires, Argentina.*

² *NCAR, P.O. Box 3000, Boulder, Colorado 80307-3000, U.S.A.*

(Dated: June 3, 2019)

We derive statistical equilibrium solutions of the truncated inviscid surface quasi-geostrophic (SQG) equations, and verify the validity of these solutions at late times in numerical simulations of the truncated SQG equations. The results indicate enstrophy thermalizes while energy can condense at the gravest modes, in agreement with previous indications of a direct cascade of enstrophy and an inverse cascade of energy in forced-dissipative SQG systems. At early times, the truncated inviscid SQG simulations show a behavior reminiscent of forced-dissipative SQG turbulence, and we identify spectral scaling laws for the energy and enstrophy spectra. Finally, a comparison between viscous and inviscid simulations allows us to identify free-decay similarity laws for the enstrophy in SQG turbulence at very large Reynolds number.

I. INTRODUCTION

Classical Gibbs ensemble methods have been extensively applied to Galerkin representation of turbulent systems, and many examples can be found in the literature. The first studies of the statistical mechanics of discrete distributions of vortices in a two-dimensional (2D) flow using a Hamiltonian formalism can be found in [1]. Later, it was shown [2] that Gibbsian statistical mechanics can be applied to Galerkin truncations of the hydrodynamic and magnetohydrodynamic (MHD) equations. This allowed many studies of continuous vorticity distribution in truncated 2D inviscid flows [3–6], where absolute equilibrium spectra for the quadratic conserved quantities of the system were derived. Following [3], in [7] the absolute inviscid equilibrium ensemble for three-dimensional (3D) Euler flows was considered. Later, 3D inviscid magnetohydrodynamic MHD equilibrium solutions were investigated in [8], and recently the approach was extended to Hall-MHD in [9]. Other problems studied in this framework include geophysical flows [10], fast rotating flows [11, 41], and formulations of one- and two-layer quasi-geostrophic models [13].

In the absolute equilibrium, fields have Gaussian statistics and the quadratic conserved quantities of the system have associated temperatures that can be positive or negative. In the former case, the quantity is said to “thermalize”, and the quantity in the equilibrium is equally distributed among all modes in the system. In the latter case the quantity “condenses,” and is accumulated at the gravest modes. However, forced-dissipative turbulent systems are far from equilibrium, as the effect of viscosity prevents relaxation towards a true equilibrium state, giving rise to solutions with non-zero flux (cascades) and making direct comparison with equilibrium solutions inadequate. In spite of this, Gibbs ensemble methods proved useful to predict the direction of the cascades in forced-dissipative systems, depending on whether the quantity of interest thermalized or condensed in the associated truncated inviscid system (see,

e.g., [4, 7, 10, 14]).

The recent finding of transients and quasi-stable states in truncated inviscid flows, in which non-thermalized modes behave as in the viscous case (see, e.g., [15–18]), has renewed interest in classical Gibbs ensembles, indicating more information than just the direction of the cascades can be extracted from these systems. In particular, it was found that at early times and as the system evolves towards equilibrium, a comparison between the inviscid system and a viscous turbulent flow can be achieved by considering in the inviscid system the net effect of the modes that have already thermalized as an effective viscosity acting on the non-thermalized modes [16, 17]. This viscous-like dynamics was reported in many systems, including the 3D truncated Euler equation [15–17], 3D truncated rotating flows [41], 2D truncated MHD [19], and turbulent Bose-Einstein condensates (BEC) using the truncated Gross-Pitaevskii equations [20]. In this latter case, the truncated equations allowed the study of thermalization of BEC at finite temperature.

Classical Gibbs ensembles and quasi-stable states were also used to study the behavior of atmospheric models (see, e.g., [21]), as the need to study atmospheric and oceanic flow dynamics has led to a variety of approximate models derived from the 3D Navier-Stokes equation for stratified and rotating flows (see for example [22–24]). In the often used geostrophic approximation, the vertical component of the velocity field is assumed zero ($u_z = 0$), and hydrostatic balance is solved in that direction while a linear balance between the Coriolis force and the pressure gradient is solved on the horizontal plane. Another family of models is given by the so-called quasi-geostrophic (QG) models, which are a first order departure of the linear geostrophic balance on the horizontal plane. A particular case of the QG models is the Surface Quasi-Geostrophic (SQG) approximation [25–30], which describes rotating stratified flows with constant potential vorticity. In this model, the vertical gradient of the stream function ψ matches a scalar field (the density field ρ or the potential temperature T) at a flat sur-

face $z = 0$. The scalar field is identified with the horizontal Laplacian $(-\nabla)^{1/2}\psi$, and the equation for the advection of this scalar by the incompressible surface flow $\mathbf{u} = \nabla\psi \times \hat{z} = (-\partial_y\psi, \partial_x\psi, 0)$ is solved. Contrary to three-dimensional QG turbulence whose dynamics is driven by large-scale interior potential vorticity gradients, SQG flows are entirely driven by density or potential temperature variations at the surface. Recently, this system has been used to study the dynamics of the upper troposphere [31–33], and of the upper oceanic layers with relative accuracy down to 500 meters [34–36]. Turbulence in forced-dissipative SQG systems (including direction of cascades and scaling laws) has also been studied in numerical simulations [25, 29, 30].

In this paper we investigate the classical Gibbs ensemble solution of the truncated inviscid SQG equations, and compare these solutions and their viscous-like transient with solutions of the dissipative SQG equations. In particular, we derive solutions for the energy and enstrophy equilibrium spectrum, verify numerically the convergence of the truncated SQG solutions to the statistical equilibrium solutions, and we compare inviscid and viscous numerical results. The statistical equilibrium solution indicates enstrophy thermalizes and energy condenses in SQG, in agreement with previous numerical results where a direct cascade of enstrophy and an inverse cascade of energy were reported [25, 37]. In the viscous-like transient, we observe the development of inertial ranges with $\sim k^{-5/3}$ scaling for the enstrophy spectrum. Finally, we present a new analogy between the non-thermalized fraction of the energy and enstrophy in the inviscid truncated runs, and the similarity free decay of the same quantities in the viscous SQG equations at very large Reynolds number.

The paper is organized as follows. In Sec. II we introduce the SQG equations and derive the statistical equilibrium solutions using the canonical distribution function formalism. In Sec. III we present a set of numerical simulations of the truncated inviscid SQG equations. We first compare them with the theoretical equilibrium solutions, and we then introduce a viscous SQG system comparing the time evolution of viscous and inviscid simulations. Finally, we present our conclusions in Sec. IV.

II. SQG AND THE GIBBS ENSEMBLE

The system considered in this paper is an incompressible two-dimensional SQG flow. Its equations are usually presented in the literature as part of a family of equations governing the advection of a scalar [25]

$$q = (-\nabla)^{\alpha/2}\psi. \quad (1)$$

This family includes the SQG equations ($\alpha = 1$, which is the case in the present study) [26, 38], the vorticity equation in an Euler flow ($\alpha = 2$), and the equation of motion for a shallow flow in a rotating domain driven by uniform internal heating ($\alpha = 3$) [28]. The case $\alpha = -2$

corresponds to a shallow-water QG equation in the limit of large length scales compared to the deformation scale (see [39]).

The flow in these models is described by a stream function ψ , and governed by the so-called α -turbulence equations which are usually written in the general form

$$\partial_t q + J(q, \psi) = 0, \quad (2)$$

where J is the Poisson bracket

$$J(A, B) = \partial_x A \partial_y B - \partial_x B \partial_y A. \quad (3)$$

For SQG, Eq. (1) in Fourier space reduces to $\hat{q}(\mathbf{k}) = -|\mathbf{k}|\hat{\psi}(\mathbf{k})$, and Eq. (2) reads

$$\partial_t \hat{\psi} = \frac{1}{|\mathbf{k}|} \left(\widehat{\partial_x q \partial_y \psi} - \widehat{\partial_x \psi \partial_y q} \right), \quad (4)$$

where the hats denote Fourier transformed. SQG dynamics possesses two quadratic conserved quantities, analogous to energy and enstrophy in two-dimensional Euler flows, which are defined respectively as

$$E = -\frac{1}{A} \int q\psi \, dx dy, \quad (5)$$

and

$$G = \frac{1}{A} \int q^2 \, dx dy, \quad (6)$$

with A the total area of the integration domain.

Note in the forced-dissipative case, the Kolmogorov-Batchelor-Kraichnan theory predicts two inertial ranges for these quantities [25]: an inverse energy cascade with spectra $E(k) \sim k^{-2}$ and $G(k) \sim k^{-1}$, and a direct enstrophy cascade with spectra $E \sim k^{-8/3}$ and $G \sim k^{-5/3}$. We will consider this case in Sec. III.

Writing $k = |\mathbf{k}|$, the energy and enstrophy of each Fourier mode \mathbf{k} are easily related by

$$G(\mathbf{k}) = kE(\mathbf{k}) = |\hat{u}(\mathbf{k})|^2. \quad (7)$$

Since $\hat{u}_x(\mathbf{k}) = ik_y \hat{\psi}(\mathbf{k})$, $\hat{u}_y(\mathbf{k}) = -ik_x \hat{\psi}(\mathbf{k})$, and the relation between the energy in each mode and the potential is

$$|\hat{u}|^2 = (k_x^2 + k_y^2)|\hat{\psi}|^2 = k^2|\hat{\psi}|^2, \quad (8)$$

the energy and enstrophy can then be written in Fourier space as follows

$$E = \sum_{\mathbf{k}/k \in N'} k |\hat{\psi}(\mathbf{k})|^2, \quad (9)$$

$$G = \sum_{\mathbf{k}/k \in N'} k^2 |\hat{\psi}(\mathbf{k})|^2, \quad (10)$$

where $N' = \{1, \dots, N/2\}$ runs over all degrees of freedom of the system.

From these relations we can derive the statistical equilibrium solutions for the inviscid truncated SQG system. The generalized Gibbs canonical distribution is

$$P = \frac{1}{Z} e^{-(\beta E + \gamma G)}, \quad (11)$$

where

$$Z = \int_{\text{phase space}} e^{-(\beta E + \gamma G)} d\xi, \quad (12)$$

is the partition function and $d\xi = \prod_k du_1(\mathbf{k}) du_2(\mathbf{k})$; u_1 and u_2 are defined such that $\hat{\mathbf{u}}(\mathbf{k}) = u_1(\mathbf{k}) + iu_2(\mathbf{k})$ and are related by the incompressibility condition $\nabla \cdot \mathbf{u} = 0$ (or $\mathbf{k} \cdot \hat{\mathbf{u}} = 0$ in Fourier space) by

$$k_x \hat{u}_1 + k_y \hat{u}_1 = 0, \quad (13)$$

$$k_x \hat{u}_2 + k_y \hat{u}_2 = 0. \quad (14)$$

From Eqs. (8), (9), and (10),

$$E = \sum_{\mathbf{k}/k \in N'} \frac{|\hat{\mathbf{u}}(\mathbf{k})|^2}{k}, \quad (15)$$

$$G = \sum_{\mathbf{k}/k \in N'} |\hat{\mathbf{u}}(\mathbf{k})|^2, \quad (16)$$

and the partition function results

$$\begin{aligned} Z &= \int_{\text{phase space}} e^{-\beta \sum \frac{|\mathbf{u}(\mathbf{k})|^2}{k} - \gamma \sum |\mathbf{u}(\mathbf{k})|^2} \prod du_1(\mathbf{k}) du_2(\mathbf{k}) \\ &= \prod_{\mathbf{k}/k \in N'} \int_{\text{phase space}} e^{-|u_1(\mathbf{k})|^2 (\frac{\beta}{k} + \gamma)} |u_1| du_1(k) \times \\ &\quad \times \int_{\text{phase space}} e^{-|u_2(\mathbf{k})|^2 (\frac{\beta}{k} + \gamma)} |u_2| du_2(k). \end{aligned} \quad (17)$$

Using

$$\int_0^\infty e^{x^2 (\frac{\beta}{k} + \gamma)} x dx = \frac{k}{2(\gamma k + \beta)}, \quad (18)$$

which holds provided $Re(\gamma + \beta/k) > 0$, the partition function results

$$Z = \prod_{k \in \{1, \dots, N/2\}} \left[\frac{k}{2(\gamma k + \beta)} \right]^2. \quad (19)$$

From the partition function we can derive the energy and enstrophy mean modal intensity spectra

$$E(\mathbf{k}) = -\frac{\partial \ln Z}{\partial \beta} = \frac{2}{\gamma k + \beta}, \quad (20)$$

$$G(\mathbf{k}) = -\frac{\partial \ln Z}{\partial \alpha} = \frac{2k}{\gamma k + \beta}. \quad (21)$$

These spectra give the energy and enstrophy in each mode \mathbf{k} , and are functions of its modulus only. The usual isotropic spectrum is obtained by integrating Eqs. (20) and (21), resulting, e.g., $E(k) = \pi k E(\mathbf{k})$ provided the modes are dense enough over the entire spectrum [5]. We then finally get the expressions for the isotropic energy and enstrophy spectra,

$$E(k) = \int E(\mathbf{k}) k d\psi = \pi k E(\mathbf{k}) = \frac{2\pi k}{\gamma k + \beta}, \quad (22)$$

$$G(k) = \int G(\mathbf{k}) k d\psi = \pi k G(\mathbf{k}) = \frac{2\pi k^2}{\gamma k + \beta}. \quad (23)$$

The energy and enstrophy are quadratic magnitudes and therefore Eqs. (22) and (23) must be positive. The relation $\gamma k > -\beta$ must apply to every value of k , and as the case $k = 1$ is the more restrictive, we simply need the system to satisfy the condition

$$\gamma > -\beta. \quad (24)$$

This condition is enough for integral (18) to converge. Furthermore, asking the total energy and enstrophy to be positive, it is obtained that $\gamma > 0$ and the enstrophy thermalizes.

A truncated inviscid SQG system is expected to reach at large times the absolute equilibrium solutions (22) and (23). The values of γ and β are uniquely determined by the total amount of energy and enstrophy contained in the initial conditions, and can be calculated solving the system of equations

$$E(t=0) = \sum_k \frac{2\pi k}{\gamma k + \beta}, \quad (25)$$

$$G(t=0) = \sum_k \frac{2\pi k^2}{\gamma k + \beta}. \quad (26)$$

III. NUMERICAL RESULTS

In this section we present numerical simulations of the SQG equations. We first compare the inviscid spectra at late times stemming from the simulations with the results derived above. Then, we study the transition from the initial condition towards the equilibrium spectrum in simulations at larger spatial resolution, and compare the behavior of the non-thermalized fraction of energy and enstrophy in the inviscid runs with the energy and enstrophy in viscous runs.

A. Inviscid truncated runs

To solve numerically Eq. (4) in a 2D periodic domain of length 2π , we use a parallel pseudospectral code

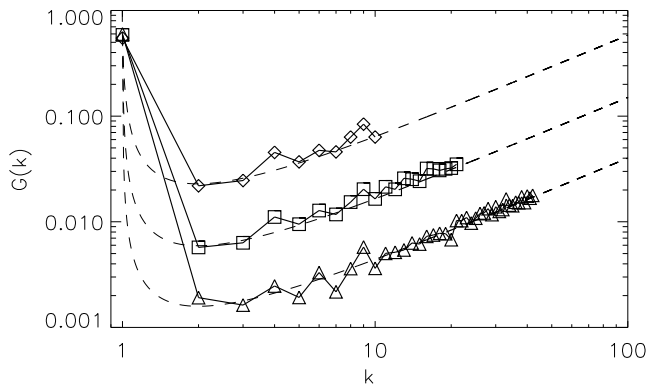


FIG. 1: Isotropic enstrophy spectra for runs with $N = 32$ (diamonds), 64 (squares), and 128 (triangles) grid points at $t = 20, 1000,$ and 24000 respectively. The Gibbs ensemble prediction (23) for each run is shown in dashed lines. Theoretical and numerical results are in good agreement for all wavenumbers.

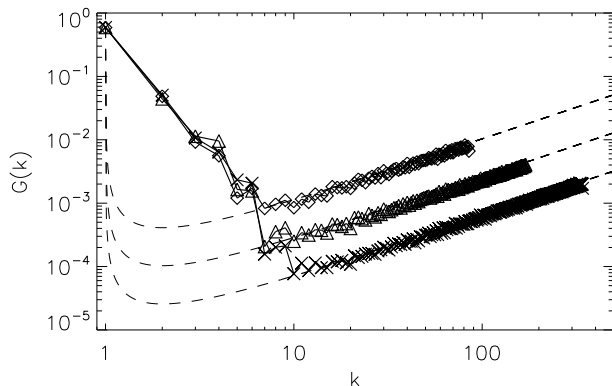


FIG. 2: Isotropic enstrophy spectra at $t = 200$ for runs with $N = 256$ (diamonds), 512 (triangles), and 1024 (crosses). The Gibbs ensemble prediction (23) is shown in dashed lines. As the resolution increases, it takes longer times for the equilibrium at large scales to be reached, while thermalization at large wavenumbers is achieved fast.

[40, 41]. Second order Runge-Kutta is used to evolve in time, and non-linear terms are computed with the 2/3-rule for dealiasing, so that the Fourier space is truncated at the maximum wavenumber $k_{max} = N/3$, with N the linear resolution. Under these conditions, pseudospectral methods are known to be equivalent to Galerkin spectral methods [42], and all quadratic invariants of the original equations are conserved in the truncated Fourier space. As an example, in simulations of the inviscid SQG equations with resolution of 512^2 grid points and a time step of $\Delta t = 2 \times 10^{-4}$, the energy was conserved up to the fourth digit after 500 turnover times.

Spatial resolutions ranged from 32^2 to 1024^2 grid points. The initial condition for all runs is a superpo-

sition of Fourier modes with random phases, with an energy spectrum $E(k) \sim k^{-2}$ for $1 \leq k \leq 4$, and zero otherwise. All simulations behave in a similar fashion, showing a progressive thermalization of modes with higher wavenumber and reaching equilibrium for long times; however, simulations at larger resolution take longer time to reach equilibrium at all scales. Once the system reaches equilibrium, its spectra should be compatible with solutions (22) and (23). To compare simulation results with the theoretical predictions, γ and β were determined solving the set of Eqs. (25) and (26) for each spatial resolution separately.

Numerical results for the isotropic enstrophy spectrum once the equilibrium was reached are shown in Fig. 1, with different symbols for the numerical data, and with dashed lines for the theoretical predictions. Numerical spectra are in good agreement with the theory at all wavenumbers, and the spectrum shows a peak at $k = 1$ (associated with the condensation of energy at the gravest modes), and a $\sim k$ scaling (associated with the thermalization of enstrophy) for larger wavenumbers. However, note that as resolution is increased, the time to reach the equilibrium increases rapidly (the spectrum for the run with 128^2 grid points is shown at $t = 24000$).

Results for higher resolutions (from 256^2 to 1024^2 grid points) at $t = 200$ together with their theoretical predictions are shown separately in Fig. 2. For higher resolutions, the thermalization process is slower and convergence of lower wavenumber modes to the statistical equilibrium solution takes progressively longer times. Nevertheless, numerical and theoretical results agree well for intermediate to high wavenumbers.

Simulations at lower resolution provide as a result a faster way to verify the validity of the Gibbs ensemble prediction. However, to study the viscous-like transient that develops as the system evolves towards equilibrium, the runs with larger resolutions will allow us better identification of scaling laws and comparison with viscous runs. We therefore focus in the following on the 1024^2 run. Figures 3 and 4 show the time evolution of the energy and enstrophy spectra in this run. At early times both spectra develop a viscous-like inertial range, with slopes compatible with Kolmogorov-Batchelor-Kraichnan phenomenology [25]. A power law $\sim k^{-5/3}$ can be identified in the enstrophy, and $\sim k^{-8/3}$ in the energy spectrum. As time evolves, the enstrophy shows a progressive thermalization starting from the largest wavenumbers, and the viscous-like inertial range becomes narrower as the $G(k) \sim k$ thermalized spectrum broadens. We will take the minimum of the enstrophy spectrum, at $k = k_{th}$, as the delimiting wavenumber between these two subranges. The flat energy spectrum for $k > k_{th}$, and its peak at $k = 1$, evidences a condensation of this quantity at low k rather than a thermalization at high wavenumbers.

In the following we define the thermalized energy and enstrophy respectively as the sum of the energy and en-

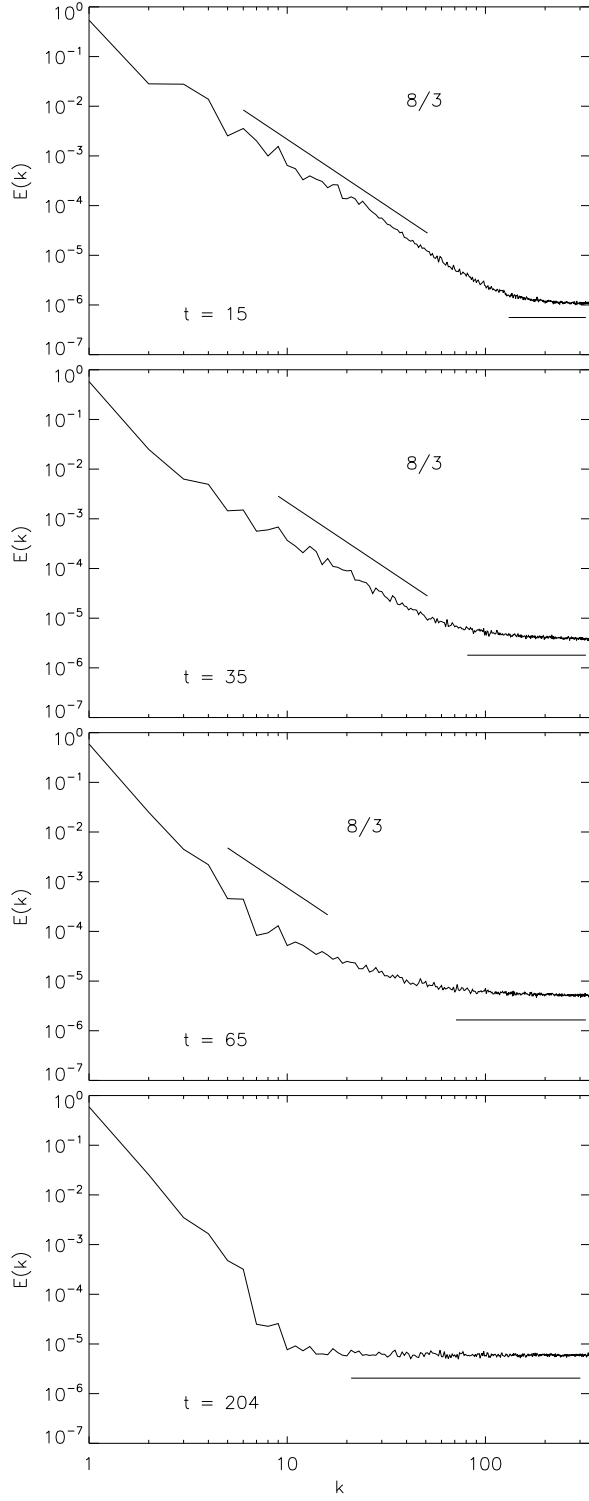


FIG. 3: Energy spectra for different times in the inviscid run with $N = 1024$. A $k^{-8/3}$ power law followed by an equilibrium subrange is observed for early times. As time evolves, more modes approach the equilibrium spectrum. The Gibbs ensemble prediction is indicated as a reference by the horizontal line.

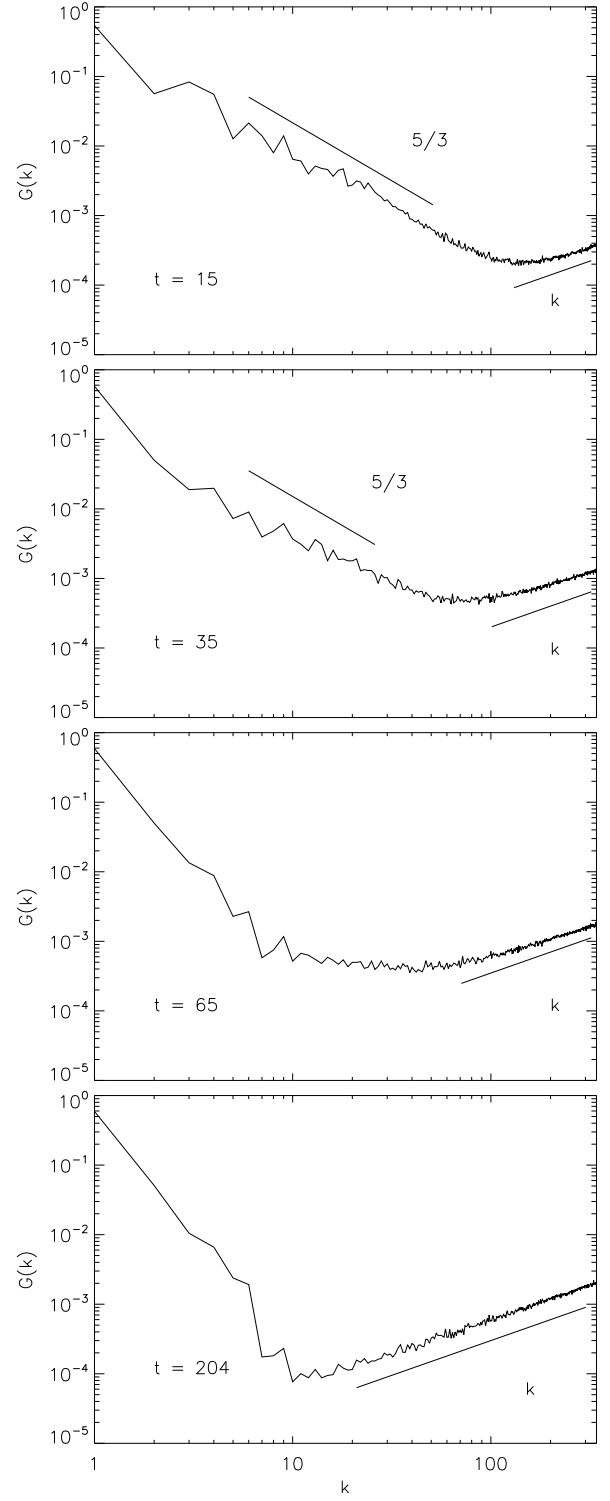


FIG. 4: Enstrophy spectra for different times in the inviscid run with $N = 1024$. A $k^{-5/3}$ power law followed by a thermalized subrange is observed for early times. As time evolves, more modes achieve thermalization. The Gibbs ensemble prediction is indicated as a reference by the $\sim k$ line.

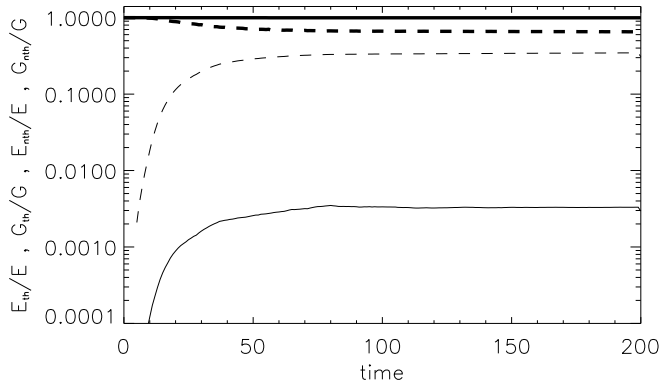


FIG. 5: Time evolution of the thermalized energy (thin solid) and enstrophy (thin dashed line) normalized by the total energy and enstrophy for the 1024^2 run. Both magnitudes grow monotonically towards their equilibrium asymptotic value. Non-thermalized energy (thick solid) and enstrophy (thick dashed) normalized respectively by total energy and enstrophy are also shown.

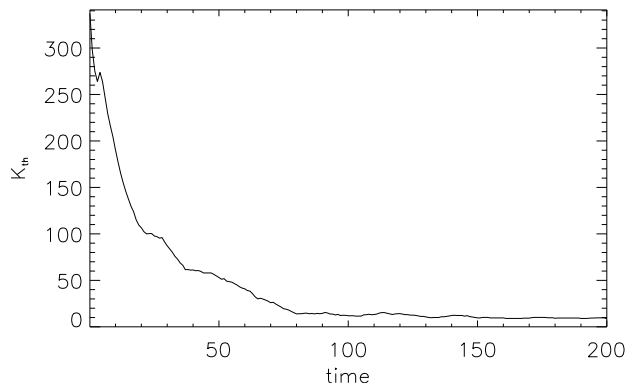


FIG. 6: Time evolution of k_{th} for the 1024^2 inviscid run. As time evolves more modes reach thermalization, but k_{th} does not converge to zero as condensation of energy takes place at the gravest modes.

strophy contained in all modes with $k \geq k_{th}$,

$$E_{th} = \sum_{k=k_{th}}^{k_{max}} E(k), \quad G_{th} = \sum_{k=k_{th}}^{k_{max}} G(k). \quad (27)$$

In a similar way, we define the non-thermalized energy and enstrophy as the difference between the total amount of these quantities (which is constant in time) and their thermalized values,

$$E_{nth} = E - E_{th}, \quad G_{nth} = G - G_{th}. \quad (28)$$

The time evolution of E_{th} , E_{nth} , G_{th} , and G_{nth} normalized respectively by E and G is shown in Fig. 5.

E_{th} and G_{th} grow monotonically at early times, converging to an almost constant value for long times. This is consistent with Figs. 3 and 4, where more and more modes approach the statistical equilibrium solution as time evolves. This is also illustrated by the evolution of k_{th} (see Fig. 6). As most of the energy condenses at $k = 1$, E_{th} remains a small fraction of the total energy while E_{nth} (which in this case represents the condensed energy) stays almost constant. On the other hand, G_{th} grows to a larger fraction of the total enstrophy as the $\sim k$ thermalized spectrum for G at large wavenumbers (see Fig. 4) holds a significant fraction of the enstrophy in the system.

As shown in Ref. [17] for the truncated Euler equations, although the truncated system is inviscid, the transfer of enstrophy towards thermalized modes before the equilibrium is reached (resulting in the growth of E_{th} and G_{th} in time) can be interpreted as a viscous-like transient in which the thermalized modes give rise to an effective viscosity acting on the non-thermalized range. This effective viscosity is responsible for the development of turbulent inertial subranges. In the next subsection we analyze in more detail this transient, comparing the inviscid system with viscous solutions.

B. Inviscid vs. dissipative systems

We focus now on the period of time when E_{th} and G_{th} are time dependent, and the flux of enstrophy towards thermalized modes can be interpreted as an out-of-equilibrium turbulent solution for $k < k_{th}$, with effective viscosity associated with the thermalized modes with $k > k_{th}$. We show that during this period, the ideal truncated model can give valuable information on the behavior of a similar but dissipative system (by similar, we mean a viscous system subject to the same initial conditions). With this aim, we compare ideal and dissipative spectra and decays for this particular period of time.

To consider dissipative SQG flows, we must solve Eq. (4) with the addition of a dissipative term,

$$\frac{\partial \hat{\psi}}{\partial t} = \frac{1}{|\mathbf{k}|} \left(\widehat{\partial_x q \partial_y \psi} - \widehat{\partial_x \psi \partial_y q} \right) - \nu |\mathbf{k}|^2 \hat{\psi}. \quad (29)$$

We solve this equation in the same way as in the ideal case, with a pseudospectral method with the 2/3-rule for dealiasing, and with second order Runge-Kutta to evolve in time.

Equation (29) in terms of the scalar q in real space reads

$$\frac{\partial q}{\partial t} = -\mathbf{u} \cdot \nabla q + \nu \nabla^2 q \quad (30)$$

Multiplying the equation by q the following conservation law follows

$$\frac{1}{2} \frac{\partial q^2}{\partial t} = \frac{1}{2} \nabla \cdot (q^2 \mathbf{u}) + \frac{1}{2} \nu \nabla^2 q^2. \quad (31)$$

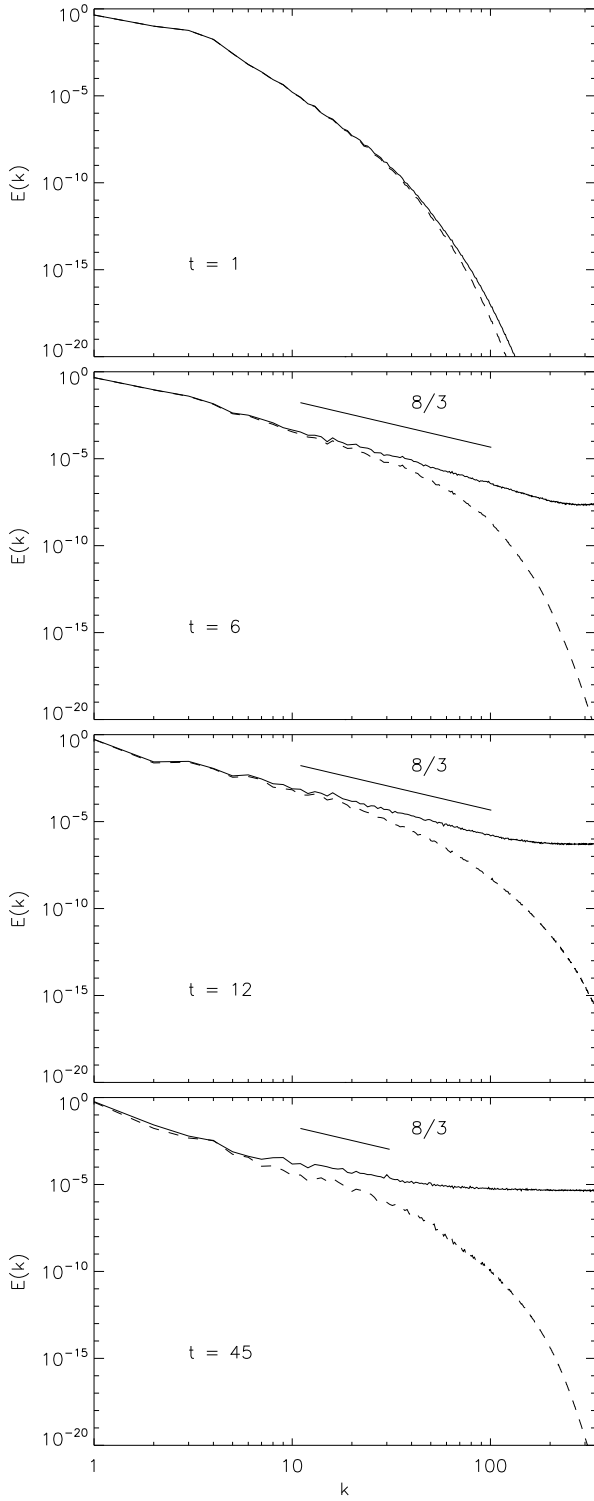


FIG. 7: Energy spectra at different times for 1024^3 inviscid (solid) and viscous (dashed) runs. Both runs develop a power law compatible with $\sim k^{-8/3}$ (indicated as a reference by the straight line). Later on, the spectra differ at intermediate and large wavenumbers, with the gravest modes still showing similar behavior.

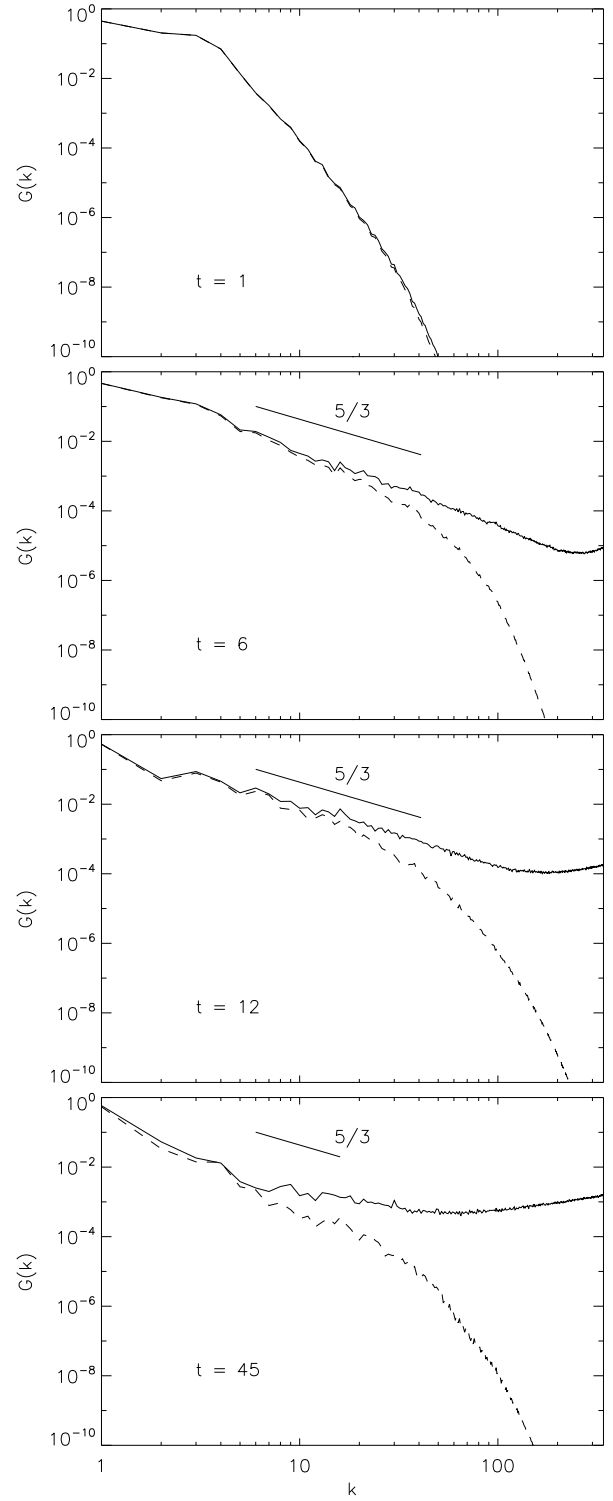


FIG. 8: Entropy spectra at different times for the same 1024^3 inviscid (solid) and viscous (dashed) runs shown in Fig. 7. A $\sim k^{-5/3}$ slope is shown as a reference.

Integrating over the entire domain, the first term on the r.h.s. cancels and Eq. (31) in Fourier space results

$$\frac{dG}{dt} = \frac{d}{dt} \int_0^\infty G(k) dk = -\nu \int_0^\infty k^2 G(k) dk = \sigma \quad (32)$$

with σ the enstrophy dissipation rate. Introducing a dissipation wavenumber k_η such that all dissipation is concentrated in Fourier space between $k = 1$ and $k = k_\eta$, in the turbulent steady state we can approximate

$$\sigma \approx -\nu \int_1^{k_\eta} k^2 G(k) dk. \quad (33)$$

From the Gibbs ensemble results, we can assume a direct enstrophy cascade, and dimensional analysis for $G(k) \sim \sigma^A k^B$ then leads to

$$G(k) \sim \sigma^{2/3} k^{-5/3}, \quad (34)$$

as obtained in Ref. [25], and the energy spectrum trivially results

$$E(k) \sim \sigma^{2/3} k^{-8/3}. \quad (35)$$

Note these power laws are the ones indicated in the dissipative-like subranges in the previous section. Replacing Eq. (34) in Eq. (33) we finally get

$$k_\eta \sim \left(\frac{\sigma}{\nu^3} \right)^{1/4}. \quad (36)$$

This relation is important to fix the resolution in viscous simulations so that all relevant scales in the flow are well resolved. In practice, we want the dissipation wavenumber to be smaller than the maximum resolved wavenumber k_{max} , or in other words, we ask for the condition

$$\left[\sum_1^{k_{max}} \frac{k^2 G(k)}{\nu^2} \right]^{1/4} \leq \frac{N}{3} \quad (37)$$

to be fulfilled at all times.

In Fig. 7 we show the energy spectra at different times for the 1024^2 ideal truncated run, and for a 1024^2 well resolved viscous run with $\nu = 4 \times 10^{-4}$. At early times, the enstrophy contained at large scales is transferred to smaller scales, and is eventually affected by thermalization or by viscous dissipation in the ideal or viscous case respectively. These effects are different, as thermalization is a time dependent problem which results in a time dependent effective viscosity (see, e.g., [16, 17]), while viscosity in the dissipative run is fixed. However, the large scales of both systems are similar at low wavenumbers, with both systems developing a $\sim k^{-8/3}$ energy power law in accordance with the theoretical results (although this subrange is wider at early times in the inviscid truncated run). This power law is lost at later times in the inviscid run, although the gravest modes still show

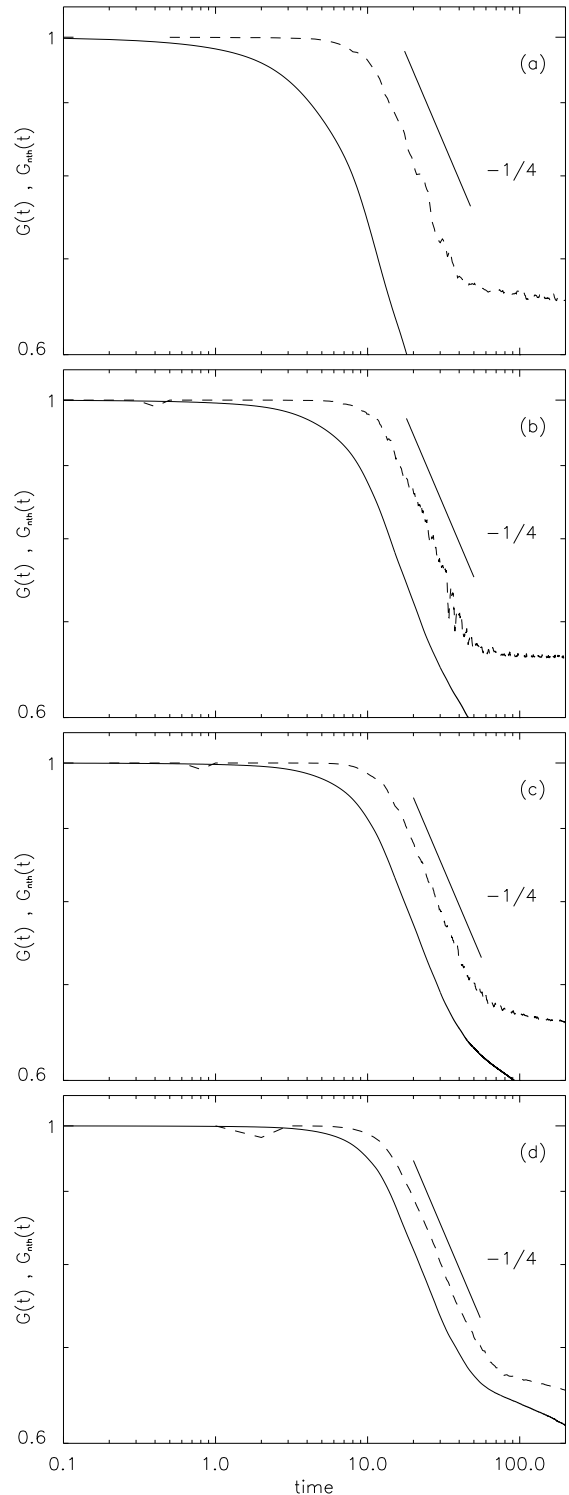


FIG. 9: Enstrophy decay $G(t)$ in viscous runs (solid line) and time evolution of $G_{nth}(t) = G - G_{th}(t)$ in ideal truncated runs (dashed lines) at increasing resolution: (a) $N = 128$, (b) $N = 256$, (c) $N = 512$, and (d) $N = 1024$. The viscous $G(t)$ approaches $G_{nth}(t)$ as the Reynolds number is increased. A $\sim t^{-1/4}$ decay is indicated as a reference.

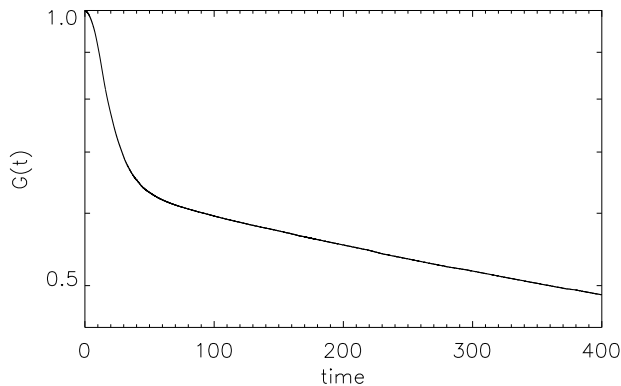


FIG. 10: Enstrophy decay $G(t)$ for a viscous run with $N = 512$ in semi-log scale. Note the exponential decay after $t \sim 50$.

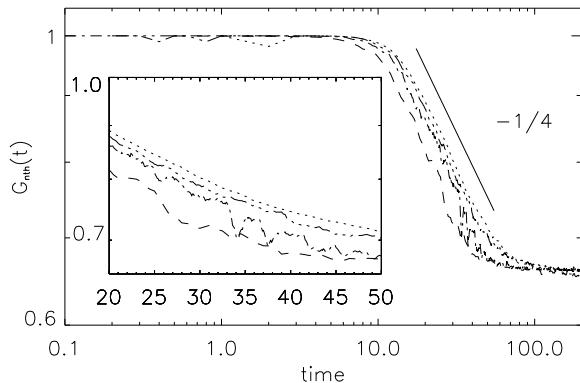


FIG. 11: Evolution of G_{nth} for different grid sizes: $N = 128$ (dashed), 256 (dash-dotted), 512 (dash-triple-dotted), and 1024 (dotted). There is small delay in the time when the decay begins as the grid size (or equivalently, k_{max}) is increased, shown in more detail in the inset. Except for this delay, all runs show the same similarity decay, with a $\sim t^{-1/4}$ decay shown as a reference.

agreement with the viscous run. A similar behavior is observed in the time evolution of the enstrophy spectrum (see Fig. 8).

The similitude in the evolution of the large scale spectra in viscous and inviscid runs makes it plausible to compare the decay of quadratic quantities in the viscous simulations, say $G(t)$, with the evolution of the associated non-thermalized quantity $G_{nth}(t)$ in inviscid truncated runs. In freely decaying turbulent flows, quadratic quantities often develop a self-similar decay law in time, once turbulence develops and dissipation sets in. The power law obeyed during the similarity decay (in this example, say, $G(t) \sim t^{-\Lambda}$) often requires large resolution as viscous effects tend to affect the decay making determination of the decay rate from the simulations difficult.

In Fig. 9, we compare the decay of the enstrophy in

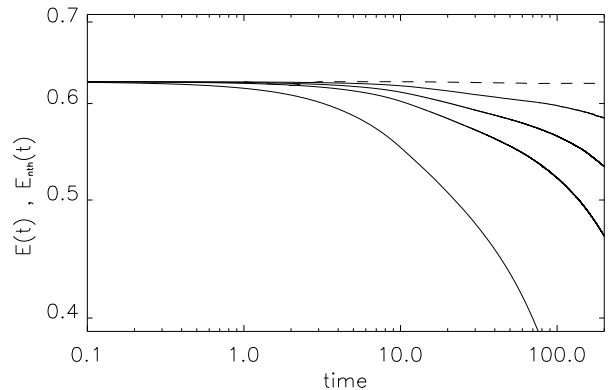


FIG. 12: Comparison between E_{nth} in an $N = 1024^2$ truncated inviscid simulation (dashed line) and $E(t)$ for viscous simulations with $N = 128$ ($\nu = 2 \times 10^{-3}$), 256 ($\nu = 5 \times 10^{-4}$), 512 ($\nu = 2.5 \times 10^{-4}$), and 1024 ($\nu = 9 \times 10^{-5}$) (bottom to top).

several dissipative runs with the evolution of $G_{nth}(t)$ in inviscid runs at different grid sizes. In all viscous cases, enstrophy is quasi-conserved at early times, and then a similarity decay develops following a power law compatible (at the largest Reynolds numbers and spatial resolution) with $G(t) \sim t^{-1/4}$. This decay is followed by a saturation and an viscous exponential decay of the enstrophy that remains in the system (see Fig. 10).

The non-thermalized $G_{nth}(t)$ in all the inviscid runs shows the same evolution, which except for a small delay in the time when the quasi-conservation is broken (see Fig. 11 and inset), is independent of the spatial resolution considered. Remarkably, the evolution of $G(t)$ seems to approach, as the Reynolds number is increased, the behavior of $G_{nth}(t)$, to the point that the decay $\sim t^{-1/4}$ can be identified in $G_{nth}(t)$ at much lower resolution (e.g., grid sizes of 128^2 or 256^2 grid points) that in the viscous run.

In this light, the decay of viscous SQG can be understood as follows. At early times, $G(t)$ remains approximately constant as the inertial range spectrum develops. As the smallest scales have not been excited yet, dissipative effects are negligible. Once turbulence develops, the similarity decay law $G(t) \sim t^{-1/4}$ is observed. The decay rate in this stage is dominated by the turbulent cascade of enstrophy towards smaller scales, and the time evolution is given by the balance equation $dG/dt = \sigma$ where the enstrophy flux σ is controlled by the non-linear term in the equation, and independent of the value of the viscosity ν as long as the Reynolds number is large enough. As a result, the truncated inviscid run, although it has a different effective viscosity, shows the same similarity decay. Later, all enstrophy that remains in the system is associated with the condensation of energy at $k = 1$, and this energy (as well as the enstrophy) can only decay exponentially in the viscous run (Fig. 10), while it remains

constant in the inviscid run (Fig. 11).

Figure 12 compares the non-thermalized fraction of the energy $E_{nth}(t) = E - E_{th}(t)$ in the $N = 1024^2$ simulation with the decay of $E(t)$ in the viscous simulations with 128, 256, 512, and 1024. In the inviscid case, as most of the energy condenses, there is no significant change in E_{nth} with time. The viscous runs approach this behavior as the viscosity is decreased, in agreement with Batchelor-Kraichnan-Leith phenomenology for systems with condensation of one invariant at large scales (see, e.g., similar arguments for the decay of the enstrophy while the energy remains approximately constant in 2D Navier-Stokes [44]).

IV. CONCLUSIONS

We derived statistical equilibrium solutions of the truncated inviscid SQG equations, and verified their validity at late times in numerical simulations of the truncated SQG equations. Numerical spectra are in agreement with the theory at all wavenumbers, although as resolution is increased it takes longer times for the system to reach equilibrium.

We also studied the evolution towards equilibrium of the ideal runs, finding that both energy and enstrophy spectra develop a viscous-like inertial range with slopes $\sim k^{-5/3}$ and $\sim k^{-8/3}$ respectively, and compatible with Kolmogorov-Batchelor-Kraichnan phenomenology. As time evolves, the enstrophy shows a gradual thermalization of higher wavenumber modes with $G(k) \sim k$, narrowing the viscous-like inertial range. The spectrum for the energy presents a flat scaling for high wavenumbers and a peak at $k = 1$, evidencing condensation of energy at small wavenumbers instead of thermalization.

Defining G_{th} and E_{th} respectively as the enstrophy and energy contained in the thermalized modes, we studied the period of time during which these quantities are time-dependent. Through this period, the transfer of enstrophy towards thermalized modes results in a viscous-like cascade with effective viscosity associated with the thermalized modes. This allowed us to compare spectra and decay in ideal runs with runs subjected to identical initial conditions but with the addition of dissipation. The large

scales of both systems are similar and both systems develop a $\sim k^{-8/3}$ energy power law in accordance with the theoretical results. At later times, the power law is lost due to thermalization in the inviscid runs and dissipation in the viscous runs.

We compared the free decay of $G(t)$ with the time evolution of the non-thermalized $G_{nth}(t)$ in inviscid truncated runs for different grid sizes. Following an initial period of time in which the enstrophy is quasi-conserved, all viscous cases develop a similarity decay compatible with $G(t) \sim t^{-1/4}$ for the largest Reynolds numbers and spatial resolutions considered. Later in time, the decay becomes shallower and an exponential viscous decay of the remaining enstrophy follows.

With the exception of a small delay in the time when the quasi-conservation is broken, all the inviscid runs show the same evolution for the non-thermalized $G_{nth}(t)$ independently of the spatial resolution considered. The evolution of $G(t)$ approaches that of G_{nth} as the Reynolds number is increased. Remarkable, inviscid systems as small as 128^2 already give information about the free decay law expected for high Reynolds viscous systems.

This good agreement between the evolution of the non-thermalized components of the enstrophy and the energy in truncated inviscid runs at low resolution, and of the decay of energy and enstrophy in viscous runs at large resolution, further indicate a new application of inviscid simulations: that of estimating the similarity decay law followed by the viscous system at very large Reynolds number. In this light, the decay of enstrophy in SQG turbulence is compatible with $G(t) \sim t^{-1/4}$ when all initial perturbations are at the gravest modes in the system. It is unclear for the moment whether the evolution of non-thermalized quantities in other inviscid truncated system can be also used as proxies of similarity decay. This problem is left for future work.

Acknowledgments

The authors acknowledge support from PICT grant No. 2007-02211, UBACyT grant No. 20020090200692, and PIP grant No. 11220090100825.

-
- [1] L. Onsager, Nuovo Cimento Suppl. **6**, 279 (1949).
 - [2] T.D. Lee, Quart. J. Appl. Math. **10**, 69 (1952).
 - [3] R.H. Kraichnan, Phys. Fluids **10**, 1457 (1967).
 - [4] D.G. Fox and S.A. Orszag, Phys. Fluids **16**, 169 (1973).
 - [5] R.H. Kraichnan, J. Fluid Mech. **67**, 155 (1975).
 - [6] R.H. Kraichnan and D. Montgomery, Rep. Prog. Phys. **43**, 547 (1980).
 - [7] R.H. Kraichnan, J. Fluid Mech. **59**, 745 (1973).
 - [8] T. Strubling and W.H. Matthaeus, Phys. Fluids B **2**, 1979 (1990).
 - [9] S. Servidio, W.H. Matthaeus, and V. Carbone, Phys. Plasmas **15**, 042314 (2008).
 - [10] M.L. Waite and P. Bartello, J. Fluid Mech. **517**, 281 (2004).
 - [11] L. Bourouiba, Phys. Fluids **20**, 075112 (2008).
 - [12] P.D. Mininni, P. Dmitruk, W.H. Matthaeus, and A. Pouquet, Phys. Rev. E **83**, 016309 (2011).
 - [13] R. Salmon, G. Holloway, and M.C. Hendershott, J. Fluid Mech. **75**, 691 (1976).
 - [14] U. Frisch, A. Pouquet, J. Léorat, and A. Mazure, J. Fluid Mech. **68**, 769 (1975).
 - [15] C. Cichowlas, P. Bonaiti, F. Debbasch, and M. Brachet,

- Phys. Rev. Lett. **95**, 264502 (2005).
- [16] G. Krstulovic, P.D. Mininni, M.E. Brachet, and A. Pouquet, Phys. Rev. E **79**, 056304 (2009).
- [17] G. Krstulovic and M.E. Brachet, Physica D **237**, 2015 (2008).
- [18] U. Frisch, S. Kurien, R. Pandit, W. Pauls, S.S. Ray, A. Wirth, and J.-Z. Zhu, Phys. Rev. Lett. **101**, 144501 (2008).
- [19] G. Krstulovic, M. Brachet, and A. Pouquet, Phys. Rev. E **84**, 016410 (2011).
- [20] G. Krstulovic and M. Brachet, Phys. Rev. Lett. **106**, 115303 (2011).
- [21] A.J. Majda and X. Wang, *Nonlinear Dynamics and Statistical Theories for Basic Geophysical Flow* (Cambridge Univ. Press, Cambridge, 2006).
- [22] J. Pedlosky, *Geophysical Fluid Dynamics* 2nd Edition (Springer, New York, 1987).
- [23] J.G. Charney, Geophys. Publ. **17**, 3 (1948).
- [24] J.G. Charney, J. Atmos. Sci. **28**, 1087 (1971).
- [25] R.T. Pierrehumbert, I.M. Held, and K.L. Swanson, Chaos, Solitons, and Fractals **4**, 1111 (1994).
- [26] I.M. Held, R.T. Pierrehumbert, S.T. Garner, and K.L. Swanson, J. Fluid Mech. **282**, 1 (1995).
- [27] C.V. Tran and D.G. Dritschel, Phys. Fluids **18**, 121703 (2006).
- [28] C.V. Tran, Physica D **191**, 137 (2004).
- [29] C.V. Tran and J.C. Bowman, J. Fluid Mech. **526**, 349 (2005).
- [30] C.V. Tran, Physica D **213**, 76 (2006).
- [31] M. Juckes, J. Atmos. Sci. **51**, 2756 (1994).
- [32] G. Hakim, C. Snyder, and D. Muraki, J. Atmos. Sci. **59**, 2405 (2002).
- [33] R. Tulloch and K.S. Smith, Proc. Natl Acad. Sci. USA **103**, 14690 (2006).
- [34] J. Isern-Fontanet, B. Chapron, G. Lapeyre, and P. Klein, Geophys. Res. Lett. **33**, L24608 (2006).
- [35] G. Lapeyre and P. Klein, J. Phys. Oceanogr. **36**, 165 (2006).
- [36] J.H. LaCasce and A. Mahadevan, J. Mar. Res. **27**, 695 (2006).
- [37] K.S. Smith, G. Boccaletti, C. CHenning, I. Marinov, C.Y. Tam, I.M. Held, and G.K. Vallis J. Fluid Mech. **469**, 13 (2002).
- [38] W. Blumen, J. Atmos. Sci. **35**, 774 (1978).
- [39] V.D. Larichev and J.C. McWilliams, Phys. Fluids A **3**, 938 (1991).
- [40] D.O. Gomez, P.D. Mininni, and P. Dmitruk, Physica Scripta **T116**, 123 (2005).
- [41] P.D. Mininni, D. Rosemberg, R. Reddy, and A. Pouquet, Parallel Computing **37**, 316 (2011).
- [42] C. Canuto, M.Y. Hussaini, A. Quarteroni, T.A. Zang, *Spectral Methods. Fundamentals in Single Domains* (Springer, Heidelberg, 2006).
- [43] C.E. Leith, Phys. Fluids **11**, 671 (1968).
- [44] G.K. Batchelor, Phys. Fluids **12** (II), 233 (1969).